

PET imaging of α_7 nicotinic acetylcholine receptors: a comparative study of [^{18}F]ASEM and [^{18}F]DBT-10 in nonhuman primates, and further evaluation of [^{18}F]ASEM in humans

Ansel T. Hillmer¹ · Songye Li¹ · Ming-Qiang Zheng¹ · Matthias Scheunemann² · Shu-fei Lin¹ · Nabeel Nabulsi¹ · Daniel Holden¹ · Richard Pracitto¹ · David Labaree¹ · Jim Ropchan¹ · Rodrigo Teodoro² · Winnie Deuther-Conrad² · Irina Esterlis¹ · Kelly P. Cosgrove¹ · Peter Brust² · Richard E. Carson¹ · Yiyun Huang¹

Received: 27 September 2016 / Accepted: 20 December 2016 / Published online: 24 January 2017
© Springer-Verlag Berlin Heidelberg 2017

Abstract

Purpose The α_7 nicotinic acetylcholine receptor (nAChR) is implicated in many neuropsychiatric disorders, making it an important target for positron emission tomography (PET) imaging. The first aim of this work was to compare two α_7 nAChRs PET radioligands, [^{18}F]ASEM (3-(1,4-diazabicyclo[3.2.2]nonan-4-yl)-6-([^{18}F]fluorodibenzo[*b,d*]thiophene 5,5-dioxide) and [^{18}F]DBT-10 (7-(1,4-diazabicyclo[3.2.2]nonan-4-yl)-2-([^{18}F]fluorodibenzo[*b,d*]thiophene 5,5-dioxide), in nonhuman primates. The second aim was to assess further the quantification and test-retest variability of [^{18}F]ASEM in humans.

Methods PET scans with high specific activity [^{18}F]ASEM or [^{18}F]DBT-10 were acquired in three rhesus monkeys (one male, two female), and the kinetic properties of these radiotracers were compared. Additional [^{18}F]ASEM PET scans with blocking doses of nicotine, varenicline, and cold ASEM were acquired separately in two animals. Next, six human subjects (five male, one female) were imaged with [^{18}F]ASEM PET for 180 min, and arterial sampling was used to measure the parent input function. Different modeling

approaches were compared to identify the optimal analysis method and scan duration for quantification of [^{18}F]ASEM distribution volume (V_T). In addition, retest scans were acquired in four subjects (three male, one female), and the test-retest variability of V_T was assessed.

Results In the rhesus monkey brain [^{18}F]ASEM and [^{18}F]DBT-10 exhibited highly similar kinetic profiles. Dose-dependent blockade of [^{18}F]ASEM binding was observed, while administration of either nicotine or varenicline did not change [^{18}F]ASEM V_T . [^{18}F]ASEM was selected for further validation because it has been used in humans. Accurate quantification of [^{18}F]ASEM V_T in humans was achieved using multilinear analysis with at least 90 min of data acquisition, resulting in V_T values ranging from 19.6 ± 2.5 mL/cm³ in cerebellum to 25.9 ± 2.9 mL/cm³ in thalamus. Test-retest variability of V_T was $11.7 \pm 9.8\%$.

Conclusions These results confirm [^{18}F]ASEM as a suitable radiotracer for the imaging and quantification of α_7 nAChRs in humans.

Electronic supplementary material The online version of this article (doi:10.1007/s00259-017-3621-8) contains supplementary material, which is available to authorized users.

✉ Ansel T. Hillmer
ansel.hillmer@yale.edu

¹ PET Center, Yale University, PO Box 208048, 801 Howard Ave, New Haven, CT 06520-8048, USA

² Helmholtz-Zentrum Dresden-Rossendorf, Institute of Radiopharmaceutical Cancer Research, Permoserstraße 15, 04318 Leipzig, Germany

Keywords Nicotine · Nicotinic Acetylcholine Receptor · Alpha7 · PET · ASEM

Introduction

The homomeric α_7 subtype of nicotinic acetylcholine receptors (nAChRs) is a class of ligand-gated ion channels distributed throughout the brain [1]. Abnormalities of α_7 nAChRs are implicated in inflammatory processes [2], schizophrenia [3], Alzheimer's disease [4], depression [5], and substance

abuse disorders [6]. In vivo imaging of α_7 nAChRs with positron emission tomography (PET) enables noninvasive measurements of receptor availability [7], and thus provides a critical tool for investigating the role of these receptors in the basic biology underlying neuropsychiatric disorders.

The first PET radioligand used to image α_7 nAChRs in humans was [^{11}C]CHIBA-1001. However, it displayed poor specificity for α_7 nAChRs and high nonspecific uptake, resulting in low specific binding signal [8]. The second α_7 nAChR PET radioligand was [^{18}F]ASEM, which exhibited high binding potentials, dose-dependent response to α_7 nAChR blockade, and appropriate kinetic properties for imaging human subjects [9–11]. As part of the initial development of [^{18}F]ASEM, the Johns Hopkins group synthesized another α_7 nAChR compound based on the same dibenzothiophene scaffold, (7-(1,4-diazabicyclo[3.2.2]nonan-4-yl)-2-([^{18}F] fluorodibenzo[*b,d*]thiophene 5,5-dioxide), initially referred to as either [^{18}F]para-ASEM or [^{18}F]JHU82108 [9], and referred to elsewhere and here as [^{18}F]DBT-10 (see Fig. 1). Only [^{18}F]ASEM was selected for further in vivo evaluation because this initial work reported higher in vitro binding affinity and selectivity for [^{18}F]ASEM than [^{18}F]DBT-10 [12] (see Supplement A). Subsequent evaluation under different in vitro binding conditions reported that [^{18}F]DBT-10 had higher affinity and selectivity than [^{18}F]ASEM for α_7 nAChRs with similar feasibility for radiofluorination at this position (see Supplement A), thus motivating its preclinical evaluation in PET imaging studies [13]. [^{18}F]DBT-10 was found to have high uptake and binding potentials in nonhuman primates with suitable kinetic properties for in vivo quantification of α_7 nAChR availability [14].

Given the favorable properties of both [^{18}F]ASEM and [^{18}F]DBT-10, the first aim of this work was to directly compare the in vivo imaging properties of [^{18}F]ASEM and [^{18}F]DBT-10 in the same animals. Follow-up experiments further tested the sensitivity of [^{18}F]ASEM to nicotine and varenicline, two common nicotinic compounds of high interest in substance abuse disorders [15]. The second aim of this work was to present a characterization of [^{18}F]ASEM quantification in humans performed at the Yale PET Center, acquiring imaging data for up to 180 min post-injection to further assess test-retest variability of kinetic parameters.

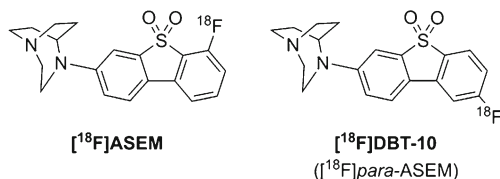


Fig. 1 Chemical structures of [^{18}F]ASEM and [^{18}F]DBT-10

Materials and methods

Radiochemistry

Production of both [^{18}F]ASEM and [^{18}F]DBT-10 was performed as previously described [14]. Briefly, both radiotracers were prepared via radiofluorination of their corresponding nitro precursors in the presence of Kryptofix-222. The crude reaction product was purified by semipreparative HPLC followed by solid-phase extraction. Subsequent formulation in 10 mL normal saline containing 1 mL ethanol followed by filter sterilization afforded the final product solution ready for dispensing and administration. Chemical purity, radiochemical purity, and specific radioactivity were determined by analytical HPLC.

Nonhuman primate imaging

Three *Macaca mulatta* animals were imaged for this study. These animals were as follows: M1, male, 6 years, 10 kg; M2, female, 15 years, 7 kg; M3, female, 16 years, 8 kg. All procedures followed institutional guidelines and were approved by the Yale University Institutional Animal Care and Use Committee.

Baseline PET scans were acquired with both [^{18}F]ASEM and [^{18}F]DBT-10 for all three subjects for a total of six scans. Three additional blocking scans were acquired with [^{18}F]ASEM in two animals, following administration of 1.84–3.13 nmol/kg (0.67–1.24 mg/kg) cold ASEM as a 15-min slow bolus starting 15–30 min before radiotracer administration. Finally, two compounds with affinity for nicotinic receptors, nicotine and varenicline (Chantix), were administered prior to PET scanning with [^{18}F]ASEM to assess its binding sensitivity to these compounds. These scans were conducted in two different animals each, with 0.24 mg/kg nicotine and 0.33 mg/kg varenicline, respectively, administered 5–10 min prior to radiotracer injection. Supplementary Table 1 summarizes the nonhuman primate imaging sessions.

Animals were first anesthetized with ketamine hydrochloride (10 mg/kg, i.m.) at least 2 h before PET scanning. Anesthesia was then maintained with 1.5–2.5% isoflurane. One catheter was placed in a saphenous vein for radiotracer administration, while a second catheter was placed in a radial or femoral artery for blood sampling. Vital signs, including respiration rate, heart rate, blood pressure, end tidal CO_2 , SpO_2 , and temperature were continuously monitored for the duration of scanning procedures.

PET data were acquired on a Focus 220 PET scanner (Siemens/CTI, Knoxville, TN, USA), which has an intrinsic resolution of 1.4 mm FWHM at the center of the field of view. Prior to radiotracer administration, a transmission scan was obtained with a rotating ^{137}Cs source over 9 min. Radiotracer ([^{18}F]ASEM or [^{18}F]DBT-10) was then

administered as a slow bolus controlled by a syringe pump (PHD 22/2000, Harvard Apparatus, Holliston, MA, USA). List-mode PET data were continuously acquired for up to 240 min. Discrete arterial blood samples were manually acquired and analyzed to measure the parent input function, as described in Supplement B, consistent with previous procedures [14]. Additionally, the free fraction (f_p) in plasma was measured with ultrafiltration cartridges (Millipore Centifree UF devices) in triplicate for each scan. The baseline [^{18}F]DBT-10 scans were previously reported [14].

To assess the specific binding of the radiotracer [^{18}F]ASEM, blocking scans using cold doses of ASEM were acquired. Additional studies using pre-blocking doses of nicotine and varenicline were conducted due to the importance of these compounds in substance use disorders, particularly tobacco smoking. Nicotine binds to $\alpha_4\beta_2$ nAChRs with high affinity ($K_i = 0.95$ nM), but has low affinity for α_7 nAChRs ($K_i = 6290$ nM) [16]. Varenicline is a partial agonist for $\alpha_4\beta_2$ nAChRs ($K_i = 0.06$ nM) and full agonist at α_7 nAChRs ($K_i = 322$ nM) with efficacy for smoking cessation [16, 17]. A table summarizing the radiotracers, blocking drug doses, and animals imaged for the blocking scans is displayed in Supplementary Table 1.

A high-resolution T1-weighted MR image was also acquired with a Siemens 3 T Trio scanner for each subject. An extremity coil was used to acquire data in the coronal direction with a spin echo sequence as follows: [echo time (TE) = 3.34 ms, repetition time (TR) = 2530 ms, flip angle = 7° , thickness = 0.50 mm, field of view = 140 mm, image matrix = $256 \times 256 \times 176$, voxel size = $0.547 \times 0.547 \times 0.500$ mm]. Non-brain structures were removed from the image using FMRIB's Brain Extraction Tool (<http://www.fmrib.ox.ac.uk/fsl/BET>).

Human imaging procedures

Six healthy volunteers (five men, one woman; 26–51 years old) were recruited from the local community. Of these six subjects, four subjects returned for a retest scan to examine the test-retest variability of [^{18}F]ASEM quantification. Written informed consent was obtained from all subjects. Subjects were screened for the following criteria: no current or history of major medical illness; no psychotropic drug use in the previous 6 months; no DSM IV Axis I diagnosis for neurological or psychiatric disorders; not pregnant or breastfeeding. Study approval and oversight was administered by the Human Investigation Committee, Yale University School of Medicine, and Yale-New Haven Hospital Radiation Safety Committee, in accordance with the Protection of Human Subjects of Research and Ethical Principle and Guidelines.

PET data were acquired with a High Resolution Research Tomograph (HRRT; Siemens/CTI; Knoxville, TN, USA).

Subjects wore an optical motion-tracking tool (Vicra, NDI Systems, Waterloo, ON, Canada) on their head to correct for motion. Imaging sessions began with the acquisition of a ^{137}Cs transmission scan over 6 min for attenuation correction. Acquisition of list-mode PET data began with the administration of 317 ± 87 MBq (range, 147–368 MBq) [^{18}F]ASEM as a slow bolus over 1 min into a forearm vein. PET data were acquired in two sessions. The first session lasted for 120 min after radiotracer injection, followed by a 30-min break where the subject left the scanner. The second session lasted from 150 min to 180 min post-injection, with a second ^{137}Cs transmission scan acquired afterwards. Blood samples were manually acquired from a radial artery to measure the metabolite-corrected arterial input function and analyzed using the same methods as in nonhuman primate experiments described above [14] and in Supplement B.

High-resolution T1-weighted MR images were acquired with a 3 T Trio MR scanner (Siemens Medical Systems, Erlangen, Germany) for each human subject prior to PET sessions. The weighted gradient-echo (MPRAGE) sequence included $TE = 3.3$ ms; $TI = 1100$ ms; $TF = 2500$ ms; $FA = 7^\circ$, resulting in a 1 mm^3 isotropic resolution. Non-brain structures were removed from the image using FMRIB's Brain Extraction Tool.

Image data processing and analysis

List-mode PET data were histogrammed into time bins up to 5 min long and reconstructed into imaging space. Nonhuman primate data from the Focus 220 were reconstructed with Fourier rebinning followed by 2-D filtered back projection with a 0.15 mm^{-1} Shepp filter. Human data from the HRRT were reconstructed with the ordered subsets expectation maximization based MOLAR algorithm, including corrections for observed subject motion [18]. For Focus 220 data, reconstructed PET images were registered to each subject's MR image using a rigid body registration algorithm [19], and the subject's MR image was subsequently normalized to a rhesus monkey MRI atlas [20]. For HRRT data, the first 10 min of PET data were summed and registered to a subject-specific MR image using a rigid mutual information algorithm (FLIRT, FSL 3.2; Analysis Group; FMRIB, Oxford, UK), and the subject's MR image was subsequently normalized to the AAL template. Both MRI normalization procedures used the nonlinear registration algorithm in BioImage Suite 3.01 (www.bioimagesuite.org/index.html). Binary template masks identifying the caudate, cerebellum, cingulate cortex, frontal cortex, hippocampus, occipital cortex, pons, putamen, temporal cortex, and thalamus were used to extract time-activity curves from these regions.

For all scans, the primary outcome measure was total distribution volume (V_T) [21]. Free-fraction corrected total distribution volumes (V_T/f_p) were also recorded. These values were

calculated in all regions with the one-tissue (1TCM) and two-tissue (2TCM) compartment models [22] and multilinear analysis method (MA1) [23]. The MA1 operational equation is:

$$C_T(t) = -\frac{V_T}{b} \int_0^t C_P(\tau) d\tau + \frac{1}{b} \int_0^t C_T(\tau) d\tau (t > t^*)$$

where C_T is the radioactivity concentration in the tissue and C_P is the parent radiotracer concentration in arterial plasma. Analyses were performed with in-house code developed in IDL. To compare model suitability, an Akaike information criterion (AIC; [24]) value was calculated for each model fit in every region. Values within each region were compared across models, and the lowest AIC value indicated a preferred model fit. MA1 was also used to estimate V_T at the voxel level to create parameterized maps for visual assessment. For the blocking scans in nonhuman primates, Lassen plots were used to estimate receptor occupancy and V_{ND} values [25].

The test-retest reproducibility of the primary outcome measure, V_T , was evaluated in each region for the four human subjects with repeated PET scans. Test-retest variability (TRV) was calculated as the difference in values between the two scans divided by the averaged values of the two scans, or $TRV = 2 * (V_{T(Test)} - V_{T(Retest)}) / (V_{T(Test)} + V_{T(Retest)})$.

Results

Nonhuman primate imaging

Radiotracers were produced with high radiochemical purity (>99%) and high specific activity at time of injection (418 ± 362 GBq/ μ mol for [18 F]ASEM; 252 ± 163 GBq/ μ mol for [18 F]DBT-10; see Supplementary Table 1).

In arterial plasma samples, HPLC analysis identified lower parent fractions of [18 F]ASEM compared to [18 F]DBT-10 for all subjects, as shown in Fig. 2a. At 120 min post-injection, parent [18 F]ASEM composed 16% of total plasma radioactivity (averaged across subjects), compared to 30% for

[18 F]DBT-10. A sample radio-HPLC trace is shown in Supplement B. Interestingly, one subject (M2) exhibited a roughly threefold higher parent fraction than the other two. This difference was consistent for both radioligands. The lower parent fraction of [18 F]ASEM resulted in lower parent concentrations in arterial plasma for this radiotracer, as shown in Fig. 2b. The free fraction (f_p) of [18 F]ASEM in plasma was similarly lower at $14.9 \pm 1.1\%$ ($n=3$) compared to that of [18 F]DBT-10 at $18.3 \pm 3.9\%$ ($n=3$).

The time courses of both radiotracers in the nonhuman primate brain were similar, as shown in Fig. 3. Kinetic analysis with compartment modeling identified the 2TCM as a better model than 1TCM for both radiotracers due to lower AIC scores across all regions. The K_1 values were high for both radiotracers, with averages of 0.59 ± 0.14 mL/cm³·min⁻¹ for [18 F]ASEM and 0.66 ± 0.11 mL/cm³·min⁻¹ for [18 F]DBT-10, respectively, across all subjects and gray matter regions. Values of k_2 were similar between the radiotracers, as indicated in Fig. 3c; 0.022 ± 0.010 min⁻¹ for [18 F]ASEM and 0.024 ± 0.010 min⁻¹ for [18 F]DBT-10. The MA1 method with $t^* = 30$ min produced V_T values consistent with those from 2TCM. Regional V_T values were higher for [18 F]DBT-10, while correcting for f_p yielded higher V_T/f_p values for [18 F]ASEM (see Fig. 3c).

Guo plots [26] directly comparing the two radiotracers (see Supplementary Figure 1) resulted in y-intercepts not significantly different from zero, indicating similar specific binding levels between the radiotracers. Estimated slopes indicated similar in vivo K_D values for the two radiotracers. Since pharmacokinetic modeling resulting in similar K_1 and k_2 estimates for these radiotracers, we conclude that [18 F]ASEM and [18 F]DBT-10 have similar in vivo properties in the rhesus monkey. Given the previous extension of [18 F]ASEM to human use [11], for consistency we elected to focus on [18 F]ASEM for further evaluation.

Subsequent preclinical experiments examined the sensitivity of [18 F]ASEM to competition with the nicotinic compounds nicotine and varenicline. No changes in [18 F]ASEM V_T values were observed due to either compound.

Fig. 2 Comparison of [18 F]ASEM and [18 F]DBT-10 in arterial plasma of nonhuman primates at baseline. **a:** Parent fractions. **b:** Arterial input functions, in SUV units

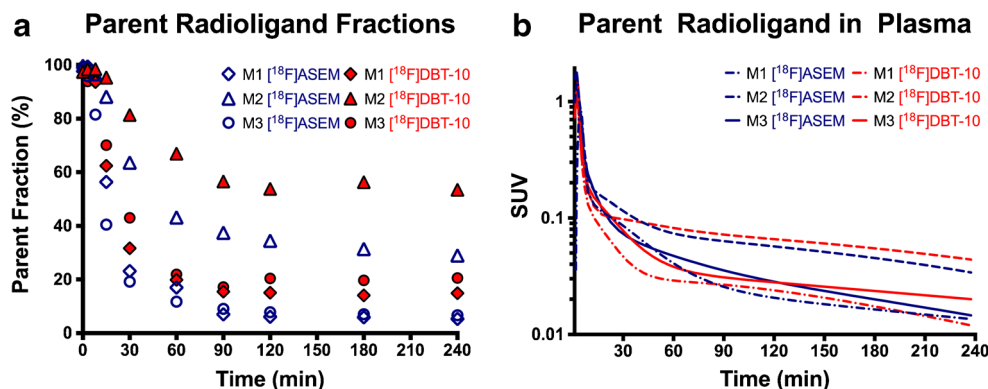
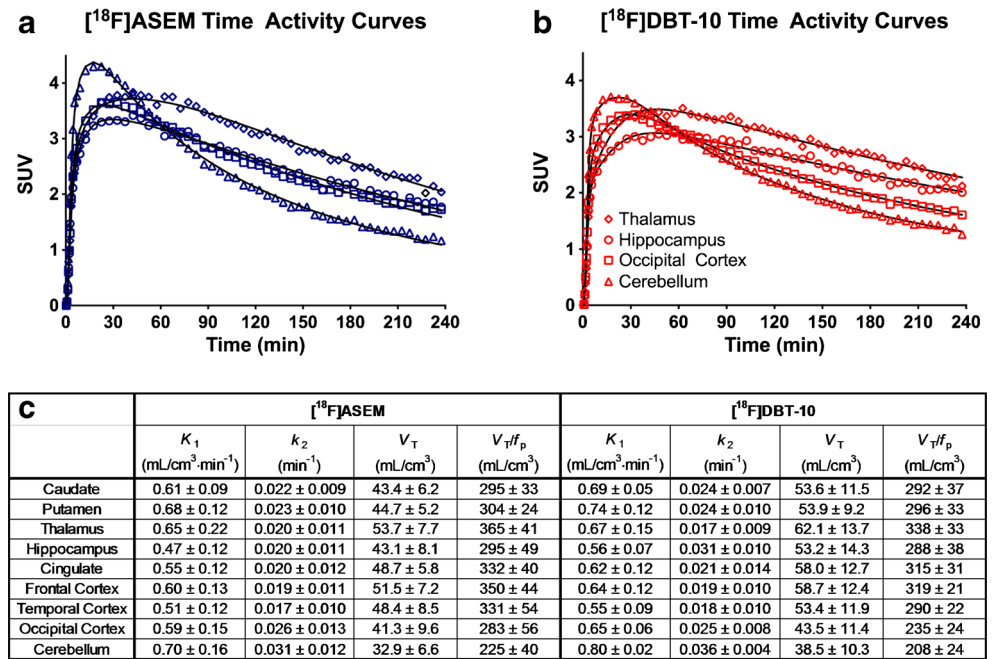


Fig. 3 Comparison of baseline [^{18}F]ASEM (a) and [^{18}F]DBT-10 (b) time-activity curves (open symbols) with the preferred 2TCM fit (solid lines). Values are expressed in SUV. c shows kinetic parameters for each radiotracer estimated with 2TCM. Values shown indicate mean \pm standard deviation



Administration of 0.24 mg/kg nicotine changed [^{18}F]ASEM V_T by $-0.1 \pm 6.7\%$ and $5.3 \pm 9.1\%$ averaged across regions for the two animals, while corresponding changes for V_T/f_p were $-7.2 \pm 6.2\%$ and $-3.0 \pm 8.4\%$. Similarly, administration of 0.33 mg/kg varenicline changed [^{18}F]ASEM V_T by $-2.6 \pm 6.2\%$ and $5.2 \pm 16.9\%$, while corresponding changes in V_T/f_p were $-1.6 \pm 5.5\%$ and $-5.4 \pm 15.2\%$. Self-block of [^{18}F]ASEM yielded a dose-dependent response, with 1.24 mg/kg ASEM inducing 36.7% and 40.2% receptor occupancy in two animals, while 0.67 mg/kg ASEM occupied 18.8% of receptors in one animal, as shown in Supplementary Figure 2A. The estimated [^{18}F]ASEM V_{ND} values were $25.3 \text{ mL}/\text{cm}^3$ and $16.0 \text{ mL}/\text{cm}^3$ for the two animals imaged.

Evaluation of [^{18}F]ASEM in humans

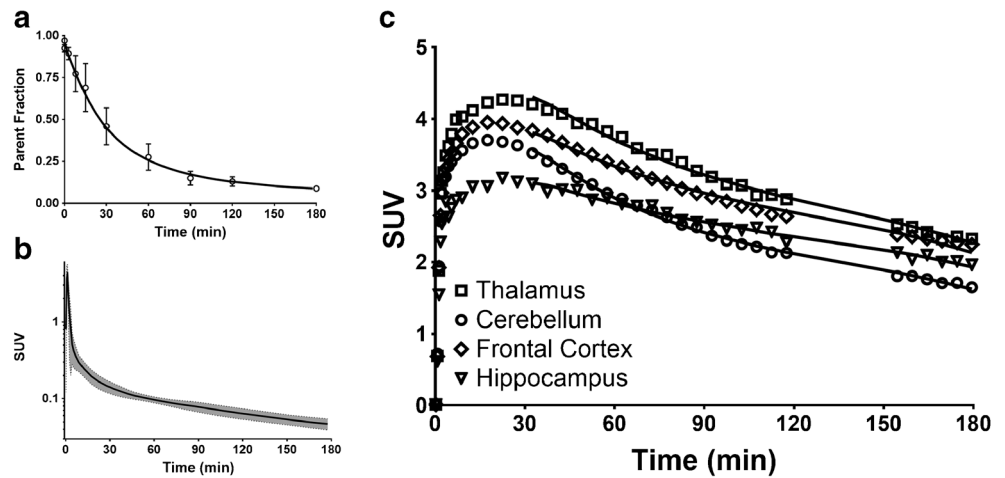
For human scans, high specific activity ($1812 \pm 404 \text{ GBq}/\mu\text{mol}$) [^{18}F]ASEM was injected, with total administered mass of $132 \pm 185 \text{ ng}$ (range, 31–654 ng; $n=10$). No detectable pharmacological effects were observed following administration of this mass dose.

Parent [^{18}F]ASEM in arterial plasma rapidly decreased following injection, as indicated in Fig. 4a. At 60 min after injection, $27.5 \pm 7.9\%$ of radioactivity in plasma was parent [^{18}F]ASEM, which further decreased to $8.8 \pm 1.6\%$ at 180 min post-injection. The parent [^{18}F]ASEM curve (shown in Fig. 4b) peaked at 1.25 min with SUV values of 4.4 ± 1.2 , and decreased to SUV values of 0.47 ± 0.08 at the end of scans (180 min post-injection). Values of f_p were $7.7 \pm 1.3\%$ ($n=6$).

In the human brain, radioactivity concentrations peaked at 20–30 min post-injection with SUV values of 3.0–4.5, and subsequently decreased in all regions (Fig. 4c). The 1TCM was well suited for [^{18}F]ASEM quantification (see sample fit shown in Supplementary Figure 3). Values of AIC for 1TCM were lower or equivalent compared to those obtained with the 2TCM (see Supplementary Table 2), and kinetic modeling of the data with 2TCM did not converge to reliable V_T estimates in hippocampus for all subjects. V_T values ranged from $20.0 \pm 3.2 \text{ mL}/\text{cm}^3$ in cerebellum to $26.6 \pm 3.3 \text{ mL}/\text{cm}^3$ in thalamus, while K_1 values ranged from $0.26 \pm 0.04 \text{ mL}/\text{cm}^3$ per min in hippocampus to $0.39 \pm 0.10 \text{ mL}/\text{cm}^3$ per min in putamen, as shown in Table 1. Use of MA1 with $t^* = 30$ min yielded comparable V_T values with 1TCM ($V_{T(\text{MA1})} = 1.02V_{T(1\text{TCM})} + 0.01$; $R^2 = 0.995$; see Supplementary Figure 4), as demonstrated in Table 1. Sample MA1 fits are shown in Fig. 4c. To explore the effects of scan duration, the 180 min of data were truncated to 120 min, 90 min, and 60 min, and V_T values were compared. Shorter data durations negatively biased V_T and increased parameter variability. Using 120 min of data underestimated V_T values by $4.2 \pm 2.6\%$ ($R^2 = 0.948$; Supplemental Figure 5A); using 90 min of data underestimated V_T by $5.5 \pm 3.8\%$ ($R^2 = 0.878$; SuppFig. 5B); using 60 min of data underestimated V_T by $7.4 \pm 5.1\%$ ($R^2 = 0.715$; SuppFig. 5C). Based on the reduced consistency of V_T estimation with 60 min of data ($R^2 = 0.715$), at least 90 min of PET data are recommended for accurate [^{18}F]ASEM V_T quantification.

Of the six subjects scanned, four returned 7–10 days later for a retest scan. Based on V_T values estimated with MA1 using 120 min of acquired PET data, test-retest variation of

Fig. 4 [¹⁸F]ASEM Kinetics in Humans. **a** shows the measured parent [¹⁸F]ASEM fractions in arterial plasma (*n* = 6; error bars are standard deviations). **b** shows the parent [¹⁸F]ASEM input functions in SUV units (*n* = 6; shaded area indicates ± 1 standard deviation). **c** shows representative [¹⁸F]ASEM time-activity curves in SUV units for four regions. Solid lines indicate fits with MA1 using *t** = 30 min



V_T was $11.7 \pm 9.8\%$. The plasma-free fraction (f_p) exhibited a test-retest variation of $-5.3 \pm 18.0\%$, and the test-retest variation of V_T/f_p was $9.3 \pm 7.3\%$. These data are summarized in Table 1. A set of V_T parametric images from the test and retest scans in a representative subject are shown in Fig. 5.

Discussion

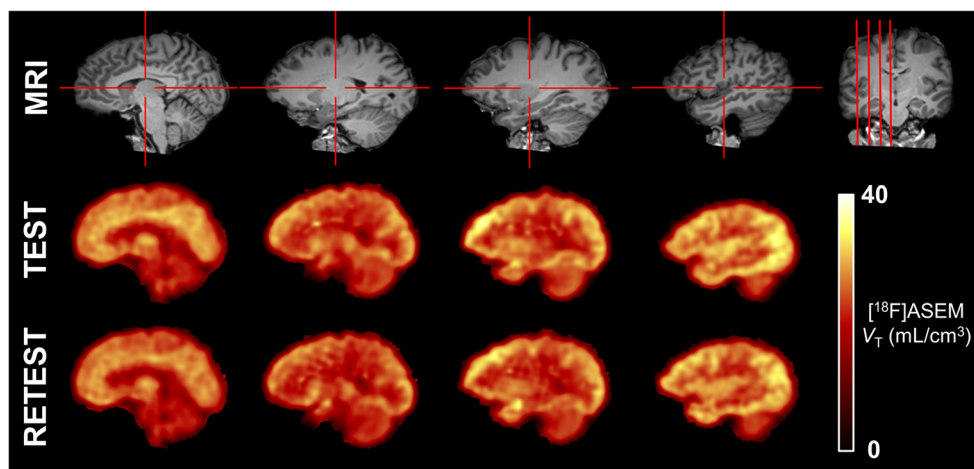
This work directly compares the in vivo kinetic properties of two PET radiotracers specific to α_7 nAChRs, [¹⁸F]ASEM and [¹⁸F]DBT-10, in nonhuman primates. Although the two radiotracers were highly similar, we selected [¹⁸F]ASEM for translation to human studies, as its use in humans has been reported previously [11]. That report indicated the need for further confirmation of [¹⁸F]ASEM test-retest variability due to the limited number of subjects in their first-in-human study [11]. This second characterization of [¹⁸F]ASEM quantification in humans identified the need for at least 90 min of data acquisition to reliably estimate V_T using MA1 analysis, yielding a test-retest variability of $11.7 \pm 9.8\%$ in four subjects.

[¹⁸F]ASEM and [¹⁸F]DBT-10 are structural isomers based on the dibenzothiophene scaffold, differing only in the position of the fluoro substituent (see Fig. 1). In contrast to initial in vitro binding results [12], further in vitro data indicated that [¹⁸F]DBT-10 had higher affinity and selectivity for α_7 nAChRs than [¹⁸F]ASEM [13] (see Supplement A), motivating our initial characterization of [¹⁸F]DBT-10 in nonhuman primates [14]. It is not unusual for a given ligand to exhibit different in vitro binding affinity values under different experimental conditions, particularly for the α_7 nAChR because there is no known conventional in vitro competition binding assay for this receptor. Different sources of receptor tissue (e.g., cell lines, brain, adrenal glands), and different radioligands (e.g., [³H] α -bungarotoxin, [³H]MLA, [¹²⁵I]iodo-MLA) are employed for this assay [27–31]. The affinities reported by Gao et al. were measured using rat cortical membranes assayed with the selective α_7 nAChR antagonist [¹²⁵I] α -bungarotoxin, while affinities reported by Teodoro et al. were measured using cloned human receptor protein expressed in a stably transfected cell line assayed with the selective α_7 nAChR antagonist [³H]methyllycaconitine

Table 1 K_1 and V_T values (*n* = 6) estimated with the one-tissue compartment model (1TCM), with V_T and V_T/f_p values (*n* = 6) and respective test-retest variability (TRV, *n* = 4) estimated with multilinear analysis (MA1) for [¹⁸F]ASEM in humans

	1TCM		MA1			
	K_1 (mL/cm ³ per min)	V_T (mL/cm ³)	V_T (mL/cm ³)	V_T TRV	V_T/f_p (mL/cm ³)	V_T/f_p TRV
Caudate	0.33 ± 0.08	22.4 ± 3.9	21.6 ± 2.6	12.5 ± 8.1%	288 ± 72	6.8 ± 7.4%
Putamen	0.39 ± 0.10	25.8 ± 3.6	25.4 ± 3.0	12.0 ± 8.1%	335 ± 66	7.8 ± 7.5%
Thalamus	0.38 ± 0.08	26.6 ± 3.3	25.9 ± 2.9	11.0 ± 6.4%	343 ± 75	6.9 ± 7.8%
Hippocampus	0.26 ± 0.04	21.7 ± 2.3	21.7 ± 2.1	10.9 ± 8.4%	287 ± 58	8.0 ± 7.8%
Front cortex	0.35 ± 0.07	24.7 ± 3.0	24.6 ± 2.7	11.0 ± 11.4%	326 ± 66	10.2 ± 7.7%
Temporal cortex	0.34 ± 0.07	26.1 ± 3.7	25.8 ± 3.2	11.8 ± 10.1%	342 ± 75	9.1 ± 7.8%
Occipital cortex	0.37 ± 0.06	25.6 ± 3.1	25.7 ± 2.7	10.5 ± 10.5%	339 ± 70	9.9 ± 8.4%
Cerebellum	0.36 ± 0.08	20.0 ± 3.2	19.6 ± 2.5	13.4 ± 7.6%	259 ± 57	7.8 ± 6.2%

Fig. 5 Parametric images of [^{18}F]ASEM V_T for a representative subject. Top row shows anatomical MRI, while middle and bottom rows show test and retest V_T images, respectively. Red lines in the coronal MRI slice indicate location of sagittal slices. Vertical red lines in sagittal MRI slices indicate location of coronal MRI slice, far right. V_T was estimated with MA1, $t^* = 30$ min with 5 mm Gaussian smoothing. The V_T scale, in units of mL/cm^3 , is shown on right



([^3H]MLA). An autoradiographic study in mouse brain comparing the distributions of α_7 nAChR binding sites for [^3H]MLA and [^3H] α -bungarotoxin showed that a small population of [^3H]MLA binding sites were insensitive to [^3H] α -bungarotoxin [32]. Thus, it is likely that the use of different radioligands for the in vitro binding experiments contributed to the conflicting reports of affinity and selectivity for α_7 nAChRs between [^{18}F]ASEM and [^{18}F]DBT-10.

Both [^{18}F]ASEM and [^{18}F]DBT-10 previously were characterized in nonhuman primates [10, 14], including ex vivo experiments confirming [^{18}F]DBT-10 as the only radioactive species in brain [14]. In this study we acquired baseline PET scans in the same rhesus monkeys for a direct quantitative comparison. Compartment modeling results indicated no differences in K_1 and k_2 parameters between the radiotracers. Guo plots [26] were then used to directly compare specific binding and in vivo affinities of the radiotracers. The y-intercept of Guo plots is related to the ratio of binding potentials (BP_{ND}), and the estimated intercepts of nearly zero indicated equivalent BP_{ND} values for the two radiotracers. The slope of Guo plots is proportional to the ratio of in vivo K_D values, and the estimated values suggested similar in vivo K_D values for the two radiotracers. Further technical considerations for analysis with the Guo plots are discussed in Supplement C. Anesthesia effects likely did not influence these studies because the same anesthesia protocol was used for the same animals, and evidence for no effects of either ketamine or isoflurane on α_7 nAChRs has been reported previously [33, 34]. Taken together, the experimental data indicate that [^{18}F]ASEM and [^{18}F]DBT10 have comparable in vivo kinetic properties, yielding no clear choice for further study. Since [^{18}F]ASEM has been used for human studies [11], we selected to focus exclusively on [^{18}F]ASEM for further evaluation.

Blocking experiments with nicotine were performed to assess the effects of this frequently used drug on [^{18}F]ASEM binding. These studies revealed that 0.24 mg/kg nicotine did

not significantly alter [^{18}F]ASEM V_T . Notably, the administered nicotine dose is roughly equivalent to the amount of nicotine present in 1–2 cigarettes. The finding that nicotine did not alter [^{18}F]ASEM V_T is not surprising, since nicotine has little functional effects on α_7 nAChRs in vitro [35] at concentrations found in cigarette smokers, and nicotine's affinity for α_7 nAChRs is two to three orders of magnitude lower than that for $\alpha_4\beta_2$ nAChRs [16, 36].

Blocking studies with a second nicotinic compound, varenicline (Chantix), were performed to assess the sensitivity of [^{18}F]ASEM specific binding to this drug, which has therapeutic efficacy for smoking cessation [37]. A dose of 0.33 mg/kg varenicline, estimated as roughly twice the therapeutic dose [38], resulted in no significant effects on [^{18}F]ASEM V_T . While varenicline has an order of magnitude higher affinity for α_7 nAChRs than nicotine [16], its affinity is still roughly three orders of magnitude lower than that of ASEM [9], and therapeutic doses of varenicline are not expected to induce functional effects on α_7 nAChRs [38]. Thus, the data suggesting no competition of 0.33 mg/kg varenicline with [^{18}F]ASEM are not unexpected. Notably, previous work described blocking of [^{18}F]ASEM uptake with 0.18 mg/kg varenicline in mice [11]. However, this work reported activity levels as % injected dose/g of tissue, which does not take into account changes in radioligand delivered to tissue from the arterial plasma under the blocking conditions. Indeed, our data indicate that varenicline administration reduced the parent [^{18}F]ASEM concentration at the end of scan by roughly 30% relative to the respective baseline values for both animals. Thus, less [^{18}F]ASEM both in blood and in tissue is an explanation consistent with both the previous report of reduced [^{18}F]ASEM uptake in tissue following varenicline administration [11] and the present report of no change in [^{18}F]ASEM V_T following varenicline administration. This finding reinforces the need of full kinetic modeling for accurate quantification of [^{18}F]ASEM binding, as previously demonstrated for [^{18}F]DBT-10 [14].

Administration of cold ASEM blocked [^{18}F]ASEM binding in a dose-dependent manner. Lassen plots indicated that 0.67 mg/kg occupied 19% of receptors, while 1.24 mg/kg ASEM induced 37–40% receptor occupancy (Supplementary Figure 2A). Using the data and methods described in Supplement D, a preliminary estimate of in vivo K_D for [^{18}F]ASEM was 9 ± 1 nM (Supplementary Figure 2B). Previous studies suggested that cold ASEM administration increased [^{18}F]DBT-10 f_p [14]; however, insufficient blood data were acquired after drug administration in the present work to assess their effects on [^{18}F]ASEM f_p . Therefore, we report V_T here as the primary outcome measure.

PET imaging of α_7 nAChRs with [^{18}F]ASEM in healthy humans was conducted with the goal of validating the optimal experimental and analysis procedures. In our hands, the parent fraction, input function, and tissue activity curves of [^{18}F]ASEM were similar to those from the first report of [^{18}F]ASEM PET imaging in humans, while values of V_T estimated here appear to be roughly 15% higher than those previously reported [11]. However, that initial report only acquired 90 min of PET scan data, while here we acquired PET data for up to 180 min post-injection.

The MA1 analysis method with at least 90 min of data was selected for V_T estimation. With our data, 2TCM did not converge to reliable parameter estimates in regions such as the hippocampus where washout of radioactivity in tissue was slower than other regions (see Fig. 4c). Further, AIC values for 1TCM were lower or equivalent to 2TCM in almost all cases (see Supplementary Table 2), indicating that 1TCM more appropriately quantified [^{18}F]ASEM kinetic parameters than 2TCM. However, structure was present in 1TCM fit residuals for areas of high uptake such as temporal or occipital cortex in some scans, indicating that the 1TCM might produce a biased result in these regions. Therefore, use of MA1 was further investigated as an alternative approach for V_T estimation across all regions. MA1 analysis produced good fits to the data and V_T values highly consistent with 1TCM results (see Supplementary Figure 4), suggesting a minimal bias from 1TCM. While 1TCM may be suitable for [^{18}F]ASEM analysis, particularly if K_1 estimation is desirable, it could underestimate V_T in future studies where high regional V_T values are obtained for [^{18}F]ASEM. Therefore, MA1 was the selected method for quantification of [^{18}F]ASEM V_T .

The appropriate scan duration with MA1 was then investigated. Our analysis indicates that modeling 60 min of [^{18}F]ASEM PET data consistently underestimated V_T values by $7.4 \pm 5.1\%$ with increased variability ($R^2 = 0.715$) when compared to values measured from 180 min of PET data. In contrast, analysis of PET data until 90 min post-injection provided good agreement with results from the full 180 min data ($R^2 = 0.878$). Thus, we believe a scan of at least 90 min duration is needed to measure [^{18}F]ASEM V_T with good precision. The test-retest variability of V_T with this method was $11.7 \pm 9.8\%$ in four

subjects, which is very similar to the $10.8 \pm 5.1\%$ test-retest variability in two subjects reported in the initial [^{18}F]ASEM human study [11].

In conclusion, this work directly compared the α_7 nAChR-specific radiotracers [^{18}F]ASEM and [^{18}F]DBT-10 in the same nonhuman primates. Since their kinetic properties were highly similar, [^{18}F]ASEM was selected for further study, as it has been used already in human studies elsewhere. Subsequent experiments indicated that [^{18}F]ASEM V_T was not affected by nicotine or varenicline, while dose-dependent self-blockade was observed. In humans, [^{18}F]ASEM V_T was accurately quantified with at least 90 min of PET data, with test-retest variability of $11.7 \pm 9.8\%$. These findings are consistent with the results from the first report of [^{18}F]ASEM PET imaging in humans, and support the future use of this radioligand for PET imaging and quantification of α_7 nAChRs in human subjects.

Acknowledgements We thank the staff at the Yale PET Center for their expert technical assistance in support of this work. This work was supported by NIH T32 DA022975, R01 DA015577, K02 DA031750, K01 MH092681, and the Veterans Affairs National Center for PTSD. The Deutsche Forschungsgemeinschaft is acknowledged for financial support (Project DE 1165/2-3). This publication was also supported by CTSA Grant Number UL1 TR000142 from the National Center for Advancing Translational Science (NCATS), a component of the National Institutes of Health (NIH). Its contents are solely the responsibility of the authors and do not necessarily represent the official view of NIH.

Compliance with ethical standards All applicable international, national, and institutional guidelines for the care and use of animals were followed. Procedures performed in studies involving animals were in accordance with the ethical standards of the Yale University Institutional Animal Care and Use Committee. All procedures performed in studies involving human participants were in accordance with the ethical standards of the institutional and/or national research committee and with the 1964 Helsinki declaration and its later amendments or comparable ethical standards. Informed consent was obtained from all individual participants included in the study. Procedures performed in studies involving human participants were in accordance with the ethical standards of the Yale University Institutional Review Board.

Funding This work was supported by NIH T32 DA022975, R01 DA015577, K02 DA031750, K01 MH092681 and the Veterans Affairs National Center for PTSD. The Deutsche Forschungsgemeinschaft is acknowledged for financial support (Project DE 1165/2-3). This publication was also supported by CTSA Grant Number UL1 TR000142 from the National Center for Advancing Translational Science (NCATS), a component of the National Institutes of Health (NIH). Its contents are solely the responsibility of the authors and do not necessarily represent the official view of NIH.

Conflict of interest The authors declare no conflict of interest.

References

- Hurst R, Rollema H, Bertrand D. Nicotinic acetylcholine receptors: from basic science to therapeutics. *Pharmacol Ther*. 2013;137(1): 22–54.

2. Kalkman HO, Feuerbach D. Modulatory effects of α_7 nAChRs on the immune system and its relevance for CNS disorders. *Cell Mol Life Sci.* 2016;73(13):2511–30.
3. Beinat C, Banister SD, Herrera M, Law V, Kassiou M. The therapeutic potential of α_7 nicotinic acetylcholine receptor (α_7 nAChR) agonists for the treatment of the cognitive deficits associated with schizophrenia. *CNS Drugs.* 2015;29(7):529–42.
4. Echeverria V, Yarkov A, Aliev G. Positive modulators of the α_7 nicotinic receptor against neuroinflammation and cognitive impairment in Alzheimer's disease. *Prog Neurobiol.* 2016;144:142–157.
5. Philip NS, Carpenter LL, Tyrkar AR, Price LH. Nicotinic acetylcholine receptors and depression: a review of the preclinical and clinical literature. *Psychopharmacology.* 2010;212: 1.
6. Brunzell DH, McIntosh JM, Papke RL. Diverse strategies targeting α_7 homomeric and $\alpha_6\beta_2^*$ heteromeric nicotinic acetylcholine receptors for smoking cessation. *Ann N Y Acad Sci.* 2014;1327:27–45.
7. Brust P, Peters D, Deuther-Conrad W. Development of radioligands for the imaging of α_7 nicotinic acetylcholine receptors with positron emission tomography. *Curr Drug Targets.* 2012;13(5):594–601.
8. Toyohara J, Sakata M, Wu J, et al. Preclinical and the first clinical studies on [^{11}C]CHIBA-1001 for mapping α_7 nicotinic receptors by positron emission tomography. *Ann Nucl Med.* 2009;23(3):301–9.
9. Horti AG. Development of [^{18}F]ASEM, a specific radiotracer for quantification of the α_7 -nAChR with positron-emission tomography. *Biochem Pharmacol.* 2015;97(4):566–75.
10. Horti AG, Gao Y, Kuwabara H, et al. ^{18}F -ASEM, a radiolabeled antagonist for imaging the α_7 -nicotinic acetylcholine receptor with PET. *J Nucl Med.* 2014;55(4):672–7.
11. Wong DF, Kuwabara H, Pomper M, et al. Human brain imaging of α_7 nAChR with [^{18}F]ASEM: a new PET radiotracer for neuropsychiatry and determination of drug occupancy. *Mol Imaging Biol.* 2014;16(5):730–8.
12. Gao Y, Kellar KJ, Yasuda RP, et al. Derivatives of dibenzothioephene for positron emission tomography imaging of α_7 -nicotinic acetylcholine receptors. *J Med Chem.* 2013;56(19):7574–89.
13. Teodoro R, Scheunemann M, Deuther-Conrad W, et al. A promising PET tracer for imaging of α_7 nicotinic acetylcholine receptors in the brain: design, synthesis, and in vivo evaluation of a dibenzothioephene-based radioligand. *Molecules.* 2015;20(10):18387–421.
14. Hillmer AT, Zheng MQ, Li S, et al. PET imaging evaluation of [^{18}F]DBT-10, a novel radioligand specific to α_7 nicotinic acetylcholine receptors, in nonhuman primates. *Eur J Nucl Med Mol Imaging.* 2016;43(3):537–47.
15. Nocente R, Vitali M, Balducci G, Enea D, Kranzler HR, Ceccanti M. Varenicline and neuronal nicotinic acetylcholine receptors: a new approach to the treatment of co-occurring alcohol and nicotine addiction? *Am J Addict.* 2013;22(5):453–9.
16. Coe JW, Brooks PR, Vetelino MG, et al. Varenicline: an $\alpha_4\beta_2$ nicotinic receptor partial agonist for smoking cessation. *J Med Chem.* 2005;48(10):3474–7.
17. Mihalak KB, Carroll FI, Luetje CW. Varenicline is a partial agonist at $\alpha_4\beta_2$ and a full agonist at α_7 neuronal nicotinic receptors. *Mol Pharmacol.* 2006;70(3):801–5.
18. Jin X, Mulnix T, Gallezot J-D, Carson RE. Evaluation of motion correction methods in human brain PET imaging—A simulation study based on human motion data. *Med Phys.* 2013;40(10):102503.
19. Sandiego CM, Weinzimmer D, Carson RE. Optimization of PET-MR registrations for nonhuman primates using mutual information measures: a Multi-Transform Method (MTM). *Neuroimage.* 2013;64:571–81.
20. Rohlfing T, Kroenke CD, Sullivan EV, et al. The INIA19 template and neuromaps atlas for primate brain image parcellation and spatial normalization. *Front Neuroinform.* 2012;6:27.
21. Innis RB, Cunningham VJ, Delforge J, et al. Consensus nomenclature for in vivo imaging of reversibly binding radioligands. *J Cereb Blood Flow Metab.* 2007;27(9):1533–9.
22. Gunn RN, Gunn SR, Cunningham VJ. Positron emission tomography compartmental models. *J Cereb Blood Flow Metab.* 2001;21(6):635–52.
23. Ichise M, Liow JS, Lu JQ, et al. Linearized reference tissue parametric imaging methods: application to [^{11}C]DASB positron emission tomography studies of the serotonin transporter in human brain. *J Cereb Blood Flow Metab.* 2003;23(9):1096–112.
24. Hurvich CM, Tsai C-L. Regression and time series model selection in small samples. *Biometrika.* 1989;76(2):297–307.
25. Cunningham VJ, Rabiner EA, Slifstein M, Laruelle M, Gunn RN. Measuring drug occupancy in the absence of a reference region: the Lassen plot re-visited. *J Cereb Blood Flow Metab.* 2010;30(1):46–50.
26. Guo Q, Owen DR, Rabiner EA, Turkheimer FE, Gunn RN. A graphical method to compare the in vivo binding potential of PET radioligands in the absence of a reference region: application to [^{11}C]PBR28 and [^{18}F]PBR111 for TSPO imaging. *J Cereb Blood Flow Metab.* 2014;34(7):1162–8.
27. Anderson DJ, Bunnelle W, Surber B, et al. [^3H]A-585539 [(1S,4S)-2,2-dimethyl-5-(6-phenylpyridazin-3-yl)-5-aza-2-azoniabicyclo[2.2.1]heptane], a novel high-affinity α_7 neuronal nicotinic receptor agonist: radioligand binding characterization to rat and human brain. *J Pharmacol Exp Ther.* 2008;324(1):179–87.
28. Deuther-Conrad W, Fischer S, Hiller A, et al. Assessment of α_7 nicotinic acetylcholine receptor availability in juvenile pig brain with [^{18}F]NS10743. *Eur J Nucl Med Mol Imaging.* 2011;38(8):1541–9.
29. Ettrup A, Mikkelsen JD, Lehel S, et al. ^{11}C -NS14492 as a novel PET radioligand for imaging cerebral α_7 nicotinic acetylcholine receptors: in vivo evaluation and drug occupancy measurements. *J Nucl Med.* 2011;52(9):1449–56.
30. Navarro HA, Zhong D, Abraham P, Xu H, Carroll FI. Synthesis and pharmacological characterization of [^{125}I]iodomethyllycaconitine ([^{125}I]iodo-MLA). A new ligand for the α_7 nicotinic acetylcholine receptor. *J Med Chem.* 2000;43(2):142–5.
31. Xiao Y, Abdrakhmanova GR, Baydyuk M, Hernandez S, Kellar KJ. Rat neuronal nicotinic acetylcholine receptors containing α_7 subunit: pharmacological properties of ligand binding and function. *Acta Pharmacol Sin.* 2009;30(6):842–50.
32. Whiteaker P, Davies AR, Marks MJ, et al. An autoradiographic study of the distribution of binding sites for the novel α_7 -selective nicotinic radioligand [^3H]-methyllycaconitine in the mouse brain. *Eur J Neurosci.* 1999;11(8):2689–96.
33. Udesky JO, Spence NZ, Achiel R, Lee C, Flood P. The role of nicotinic inhibition in ketamine-induced behavior. *Anesth Analg.* 2005;101(2):407–11.
34. Flood P, Ramirez-Latorre J, Role L. $\alpha_4\beta_2$ neuronal nicotinic acetylcholine receptors in the central nervous system are inhibited by isoflurane and propofol, but α_7 - type nicotinic acetylcholine receptors are unaffected. *Anesthesiology.* 1997;86(4):859–65.
35. Grottick AJ, Trube G, Corrigan WA, et al. Evidence that nicotinic α_7 receptors are not involved in the hyperlocomotor and rewarding effects of nicotine. *J Pharmacol Exp Ther.* 2000;294(3):1112–9.
36. Grady SR, Drenan RM, Breining SR, et al. Structural differences determine the relative selectivity of nicotinic compounds for native $\alpha_4\beta_2^*$ -, $\alpha_6\beta_2^*$ -, $\alpha_3\beta_4^*$ - and α_7 -nicotinic acetylcholine receptors. *Neuropharmacol.* 2010;58(7):1054–66.
37. Jorenby DE, Hays JT, Rigotti NA, et al. Efficacy of varenicline, an $\alpha_4\beta_2$ nicotinic acetylcholine receptor partial agonist, vs placebo or sustained-release bupropion for smoking cessation: a randomized controlled trial. *JAMA.* 2006;296(1):56–63.
38. Rollema H, Shrikhande A, Ward KM, et al. Pre-clinical properties of the $\alpha_4\beta_2$ nicotinic acetylcholine receptor partial agonists varenicline, cytisine and dianicline translate to clinical efficacy for nicotine dependence. *Br J Pharmacol.* 2010;160(2):334–45.